Supplementary Information

Tunable chiral spin texture in magnetic domain-walls

J. H. Franken,* M. Herps, H. J. M. Swagten, and B. Koopmans

(Dated: March 10, 2014)

* j.h.franken@tue.nl

S1. MATERIAL PARAMETERS

	M_s	K_{eff}	$\mu_0 H_D$	$\mu_0 H_K$	ϵ_{SHE}	ϵ_{calc}	ν
	MA/m	MJ/m^3	mT	mT	10^{-14} TA^{-1}m^2		
Pt(4)/Co(0.36)/Pt(1)	1.01(5)	0.39(2)	37(1)	37(1)	6.4(2)	6.7	0.68
Pt(4)/Co(0.36)/Pt(2)	1.08(5)	0.27(1)	12.5(4)	24.6(5)	2.76(6)	3.2	0.34
Pt(4)/Co(0.8)/AlOx(1.9)	1.17(5)	0.28(1)	$\gg 40$	?	4.43(6)	3.4	0.89
Pt(4)/Co(0.5)/Pt(2)	1.07(5)	0.28(1)	11(2)	37(1)	2.4(1)	2.3	0.34
Pt(2)/Co(0.5)/Pt(4)	1.18(5)	0.22(1)	3(1)	19(2)	-1.8(1)	-2.1	-0.34

Table S1. Fit parameters and material properties of various compositions.

Table S1 summarizes the measured material properties. M_s and K_{eff} have been measured by VSM-SQUID magnetometery of unpatterned films. The samples labeled with a Co thickness of 0.4 nm in the text for convenience, were actually 0.36 nm thick. $\mu_0 H_D$, $\mu_0 H_K$, and ϵ_{SHE} have been obtained by fits of the DW depinning data like in Figure 2 in the main text. Although a stronger spin Hall current is injected in Pt/Co/AlOx, ϵ_{SHE} is smaller than in Pt/Co/Pt(1 nm) because it is absorbed by a thicker Co layer (see equation (1) in the main text). The inverted stack Pt(2)/Co(0.5)/Pt(4) also has an inverted ϵ_{SHE}, as we already explained in [S1]. Figure S1 provides a new measurement of the depinning efficiency as a function of H_x on this layer system, in order to reveal the presence of DMI. There is a very small opening visible, indicative of a H_D with the same sign as the inverted composition. Actually, it seems like one of the DWs has zero H_D (crosses through the origin), whereas the other one has a small but finite H_D. In any case, this suggests that the DMI, unlike the SHE, is not a result of the Pt layer thicknesses themselves, but rather the effect of increasing asymmetry between the top and bottom interface when the top layer is varied.

Since both DMI and PMA are expectedly interface effects, it is interesting to look for correlations between the parameters H_D and K_{eff}. For the Pt/Co/Pt samples, there is indeed a positive correlation between H_D and K_{eff}. However, Pt/Co/AlOx breaks this trend: it has a much stronger H_D than any other sample whereas K_{eff} is similar, so the two parameters are definitely not always directly related. Given that the DW motion is in the direction of current flow, we know that the DMI at the bottom interface must be dominant over the DMI from the top interface [S2]. So in fact, the DMI at the top interface must *decrease* when the

top layer is made thinner, whereas the anisotropy contribution from this interface is actually seen to *increase*. So there appears to be a *negative* correlation between the anisotropy and DMI at the top interface, leading to a *positive* correlation between the anisotropy and the total DMI which is dominated by the bottom Pt/Co interface.

S1.1. Spin Hall amplitudes

In the last two columns of Table S1, we have calculated the expected loss factor ν of the spin Hall effect, and the accompanying depinning efficiency of Néel walls in the 1D model [S3],

$$\epsilon_{\mathrm{calc}} = \frac{\pi\hbar\nu\theta_{\mathrm{SH}}}{4eM_{\mathrm{s}}t}. \tag{S1}$$

The calculation of ν is straightforward; the net spin Hall current due to a *single* thin Pt layer with thickness t_{Pt} is given by [S4]

$$J_{\mathrm{S}}(t_{\mathrm{Pt}}) = \theta_{\mathrm{SH}}J\left(1 - \operatorname{sech}\left(\frac{t_{\mathrm{Pt}}}{\lambda_{\mathrm{sf}}}\right)\right), \tag{S2}$$

where $\lambda_{\mathrm{sf}} \approx 1.4\,\mathrm{nm}$ the spin diffusion length of Pt [S5] and $\theta_{\mathrm{SH}} = 0.07$ the spin Hall angle of Pt [S5]. For a Co layer sandwiched between two Pt layers, two of these spin currents with opposite polarization are injected, yielding a net spin current

$$J_{\mathrm{S}}^{\mathrm{eff}} = \nu\theta_{\mathrm{SH}}J := \left(\operatorname{sech}\left(\frac{t_{\mathrm{Pt}}^{\mathrm{top}}}{\lambda_{\mathrm{sf}}}\right) - \operatorname{sech}\left(\frac{t_{\mathrm{Pt}}^{\mathrm{bottom}}}{\lambda_{\mathrm{sf}}}\right)\right)\theta_{\mathrm{SH}}J. \tag{S3}$$

Comparing the calculated ϵ_{calc} to the measured ϵ_{SHE} in Table S1, we observe close agreement. The largest deviation is found in Pt/Co/AlOx which measures a slightly higher ϵ_{SHE} than expected. We should note that this is the only sample that has undergone an annealing treatment, hence it might have different properties compared to the other ones. There might also be a contribution from conventional STT to ϵ_{SHE} in Pt/Co/AlOx, but since conventional STT would oppose the SHE torque, this should reduce the measured ϵ_{SHE} compared to the model, whereas the difference we observe is opposite.

S2. DW RESISTANCE MODEL

In this section, we propose a model to describe the two dominant contributions to the DW resistance. We first apply the Levy-Zhang model of the intrinsic resistivity to the

expected DW profile in the sample. Then, we discuss the contribution from anisotropic magnetoresistance (AMR). Finally, an expression is given for the measured resistance change in an actual Pt/Co/Pt layer, where current shunts through the Pt layers. This expression is fitted to the experimental data.

S2.1. Levy-Zhang model for arbitrary DW profiles

The Levy-Zhang model describes the contribution to DW resistance due to spin mistracking [S6]. In their original derivation, they assume a simplified DW profile of the form $\theta(x) = \pi x/d$. However, in reality the DW has the more complicated Bloch profile, and when magnetization canting due to an in-plane field starts to play a role, the actual profile is even more complex. We therefore first derive an expression valid for any DW profile, and then insert an approximated 'canted' profile to find an expression for R_{LZ} as a function of in-plane field.

The original result of DW resistivity by Levy and Zhang for a current perpendicular to the DW reads

$$\rho_{\mathrm{LZ}} = C\left(\frac{\pi}{\lambda}\right)^2, \tag{S4}$$

with λ the DW width and C a prefactor given by

$$C = \frac{\hbar^4 k^2 \rho_0}{80 J^2 m^2}\left(\frac{\rho_\uparrow}{\rho_\downarrow} - 2 + \frac{\rho_\downarrow}{\rho_\uparrow}\right)\left(3 + \frac{10\sqrt{\rho_\uparrow/\rho_\downarrow}}{\rho_\uparrow/\rho_\downarrow + 1}\right), \tag{S5}$$

with $\hbar$ Planck's constant, $k \approx 1\mathring{A}^{-1}$ the Fermi wavevector, m the electron mass, $J \approx 0.5\,\mathrm{eV}$ the (microscopic) exchange splitting, $\rho_\uparrow/\rho_\downarrow$ the spin asymmetry in the Co layer, and ρ_0 the resistivity of the Co layer.

Eqn. (S4) was obtained for the simple DW profile with a constant slope $\mathrm{d}\theta/\mathrm{d}x = \pi/\lambda$. For a real DW in which this slope is not constant, the resistivity is position-dependent within the DW. Therefore, a more general form of the DW resistivity is

$$\rho_{\mathrm{LZ}} = C\left(\frac{\mathrm{d}\theta(x)}{\mathrm{d}x}\right)^2. \tag{S6}$$

The DW resistance is found by integrating the resistivity over the entire DW profile,

$$R_{\mathrm{LZ}}(x) = \frac{1}{S}\int_{-\infty}^{\infty} C\left(\frac{\mathrm{d}\theta(x)}{\mathrm{d}x}\right)^2 \mathrm{d}x, \tag{S7}$$

with S the cross-sectional area of the magnetic layer.

As explained briefly in the main text, we expect at high in-plane fields a DW profile that rotates from $\theta = 0$ in the non-irradiated region, to $\theta_c(H_x) < \pi$ in the Ga-irradiated region, where the anisotropy has decreased so much that the magnetization is significantly pulled in-plane. We assume a scaled Bloch profile that takes into account this smaller final angle of the DW,

$$\theta(x) = \frac{2}{\pi}\theta_c(H_x)\arctan\left(e^{x/\lambda}\right), \tag{S8}$$

where we use $\lambda = \sqrt{A/K_{\text{low}}}$ with $A = 16\,\text{pJ/m}$ and K_{low} the effective anisotropy in the irradiated region (a fit parameter), which is seen to determine the DW width in micromagnetic simulations. From the Stoner-Wohlfarth model, it is straightforward to derive that the magnetization canting as a function of in-plane field is given by

$$\theta_c(H_x) = \pi - \arcsin\left(\frac{H_x M_s}{2K_{\text{low}}}\right). \tag{S9}$$

Plugging the DW profile of Eqn. (S8) into the expression for the resistance Eqn. (S8) yields

$$R_{\text{LZ}}(H_x) = \frac{2C}{S}\frac{\left(\pi - \arcsin\left(\frac{H_x M_s}{2K_{\text{low}}}\right)\right)^2}{\pi^2\lambda}. \tag{S10}$$

Note that we used H_x in the expressions above, but the same expressions hold for H_y.

S2.2. AMR contribution

The AMR resistivity within the DW scales with the square of the projection of the magnetization on the x-axis, hence

$$\rho_{\text{DWAMR}}(x) = \rho_{\text{AMR}}\cos^2\phi\sin^2\theta(x), \tag{S11}$$

where ρ_{AMR} is the AMR resistivity parameter of Co. We will assume that the angle ϕ does not vary within the DW (which is supported by micromagnetic simulations). $\phi = 0$ represents a Néel wall, giving the highest AMR.

If there is no DW present and no canting of the magnetization, the additional AMR contribution in the presence of DWs is found by integrating Eqn. (S11). However, if one of the domains is canted in the x-direction, there is a large contribution form this domain to the AMR. This is however not the experimental situation, because the subtracted background

signal is recorded at the same in-plane field, hence AMR from the domains is not included in the presented DW resistance. Since we do not have an analytical expression for this background, we start from the original Bloch profile which rotates from 0 to π so that the integral to infinity converges, and multiply Eqn. (S11) by a correction factor $\cos^2\theta_c(H_x)$ which is not analytical but at least correct in the center of the domain wall,

$$\rho_{\mathrm{DWAMR}}(x) = \rho_{\mathrm{AMR}} \cos^2\phi \sin^2\theta(x) \cos^2\theta_c(H_x). \tag{S12}$$

Now we only need to integrate the resistivity to get the AMR contribution to the DW resistance,

$$R_{\mathrm{AMR}} = \frac{1}{S}\int_{-\infty}^{\infty} \rho_{\mathrm{DWAMR}} \mathrm{d}x = \frac{1}{S}\frac{\rho_{\mathrm{AMR}}\lambda\,(4K_{\mathrm{low}}^2 - H_x^2 M_{\mathrm{s}}^2)\cos^2\phi}{2K_{\mathrm{low}}^2}. \tag{S13}$$

S2.3. Converting to actually measured resistance change

The actually measured resistance change is reduced strongly by current shunting through the Pt layers. Assuming only a fraction $p \approx 0.03$ of the current runs through the Co layer in Pt/Co/Pt based on a Fuch-Sondheimer model [S7], the resistance of the wire R_{wire} can be described as the result of two parallel resistors $R_{\mathrm{Co}} = \frac{R_{\mathrm{wire}}}{p}$ and $R_{\mathrm{Pt}} = \frac{R_{\mathrm{wire}}}{1-p}$. The occurrence of N DWs only trigger a resistance change of the Co layer ΔR_{Co},

$$\Delta R_{\mathrm{Co}} = N(R_{\mathrm{LZ}} + R_{\mathrm{AMR}}). \tag{S14}$$

In the parallel resistor model, it is easy to show that this leads to a resistance change of the whole wire of

$$\Delta R = \frac{Np^2(R_{\mathrm{LZ}} + R_{\mathrm{AMR}})R_{\mathrm{wire}}}{R_{\mathrm{wire}} - N(p-1)p(R_{\mathrm{LZ}} + R_{\mathrm{AMR}})}. \tag{S15}$$

In the Pt(4)/Co(0.5)/Pt(2) wire, $R_{\mathrm{wire}} = 1.3\,\mathrm{k\Omega}$ and $N = 20$, whereas in the Pt/Co/AlOx wire, $R_{\mathrm{wire}} = 1.8\,\mathrm{k\Omega}$ and $N = 18$

This model for ΔR has been fitted to the DWR data in Figure 3(c) in the main text, with ρ_{AMR}, C, and K_{low} as free parameters. The value for ρ_0 in the prefactor C was calculated as $R_{\mathrm{Co}}\,S/L$, with L the length of the wire. Note that a dependence on the DW angle ϕ enters in the model via R_{AMR}. The value of ϕ at each H_x and H_y are described by minimization of Eqn. (1) in the main text, where H_D and H_K are extracted from the DW depinning data (see table S1). The best fit was obtained with parameters $\rho_{\mathrm{AMR}} = 2.9 \times 10^{-9}\,\Omega\mathrm{m}$,

$C = 2.25 \times 10^{-24}\,\Omega\mathrm{m}^3$, $K_{\mathrm{low}} = 29.8\,\mathrm{kJ/m}^3$. The value of the prefactor C implies via Eqn. (S5) that $\rho_\uparrow/\rho_\downarrow \approx 15$, which is reasonable according to the original paper by Levy and Zhang [S6]. The value for K_{low} at a dose of $0.50 \times 10^{13}\,\mathrm{ions/cm}^2$ is somewhat lower than we measured before [S8], which could relate to some of the assumptions in our modeling, such as the chosen values of the fixed parameters or the assumption that the DW width does not depend on in-plane field. Note that we did not have to include additional magnetoresistance effects such as the geometric size effect or the anisotropic interface magnetoresistance [S9] to obtain a reasonable fit. The presence of such an effect could alter the fit parameters, but our main conclusion that Bloch walls transform to Néel walls is robust simply because of the very different response to x and y fields, regardless of the precise relative magnitude of the effects that are responsible for the measured changes.

In Figure S2, we have plotted the various contributions that make up the fitted curves in Figure 3(c) (main text). The purple solid line indicates the intrinsic DW resistance as a function of in-plane field, which gives the same result for H_x and H_y fields. The dark blue dotted line shows the modeled contribution from the AMR effect under the influence of H_x fields. The light blue dash-dotted line shows a calculation of what the AMR effect would look like if we would not take into account the magnetization canting: the AMR resistance simply saturates at high H_x. The contribution from AMR as a function of H_y (dashed green curve) is quite small, and reduces at higher in-plane fields since the DW loses its slight Néel character. Note that, since we always measure DWs of both polarities in experiment, the modeled AMR under H_x fields is a superposition of two curves, mutually shifted by the chiral field $\frac{2}{\pi}H_D$.

SUPPLEMENTARY REFERENCES

[S1] Haazen, P. P. J. *et al.* Domain wall depinning governed by the spin Hall effect. *Nat. Mater.* **12**, 299 (2013).

[S2] Ryu, K.-S., Thomas, L., Yang, S.-H. & Parkin, S. Chiral spin torque at magnetic domain walls. *Nat. Nanotechnol.* **8**, 527–33 (2013).

[S3] Thiaville, A., Rohart, S., Jué, E., Cros, V. & Fert, A. Dynamics of Dzyaloshinskii domain walls in ultrathin magnetic films. *Europhys. Lett.* **100**, 57002 (2012).

[S4] Liu, L., Moriyama, T., Ralph, D. C. & Buhrman, R. A. Spin-Torque Ferromagnetic Resonance Induced by the Spin Hall Effect. *Phys. Rev. Lett.* **106**, 036601 (2011).

[S5] Liu, L., Buhrman, R. A. & Ralph, D. C. Review and Analysis of Measurements of the Spin Hall Effect in Platinum. *arXiv* **1111.3702** (2011).

[S6] Levy, P. M. & Zhang, S. Resistivity due to Domain Wall Scattering. *Phys. Rev. Lett.* **79**, 5110–5113 (1997).

[S7] Franken, J. H., Hoeijmakers, M., Swagten, H. J. M. & Koopmans, B. Tunable Resistivity of Individual Magnetic Domain Walls. *Phys. Rev. Lett.* **108**, 037205 (2012).

[S8] Franken, J. H., Hoeijmakers, M., Lavrijsen, R. & Swagten, H. J. M. Domain-wall pinning by local control of anisotropy in Pt/Co/Pt strips. *J. Phys. Cond. Matter* **24**, 024216 (2012).

[S9] Kobs, A. *et al.* Anisotropic Interface Magnetoresistance in Pt/Co/Pt Sandwiches. *Phys. Rev. Lett.* **106**, 217207 (2011).

SUPPLEMENTARY FIGURES

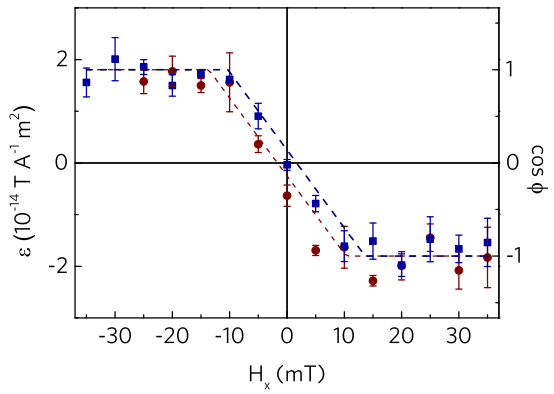

Figure S1. Depinning efficiency as a function of H_x on the inverted stack Pt(2)/Co(0.5)/Pt(4).

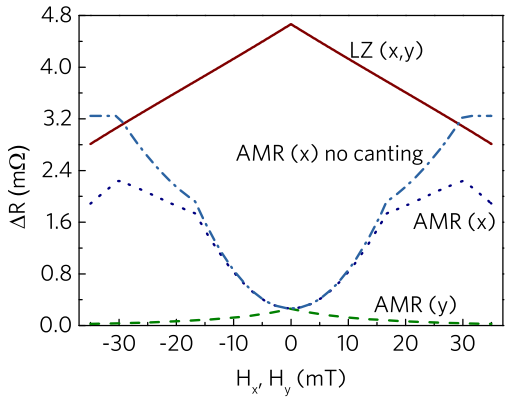

Figure S2. Contributions of the various domain wall resistance effects as a function of in-plane field. Plotted are the intrinsic Levy-Zhang contribution (solid red line), the DW AMR as a function of H_y (dashed green line) and H_x (dotted dark-blue line), and the (hypothetical) DW AMR contribution as a function of H_x in the absence of magnetization canting (dash-dotted light-blue line). The kinks occur when one of the two present domain-wall types reach the Néel state, and there are two of them on both sides because they are shifted in opposite directions by the effective chiral fields.